

Force, Impedance, and Trajectory Learning for Contact Tooling and Haptic Identification

Yanan Li [✉], *Member, IEEE*, Gowrishankar Ganesh, *Member, IEEE*, Nathanaël Jarrassé [✉],
Sami Haddadin [✉], *Member, IEEE*, Alin Albu-Schaeffer, *Member, IEEE*, and Etienne Burdet, *Member, IEEE*

Abstract—Humans can skilfully use tools and interact with the environment by adapting their movement trajectory, contact force, and impedance. Motivated by the human versatility, we develop here a robot controller that concurrently adapts feedforward force, impedance, and reference trajectory when interacting with an unknown environment. In particular, the robot's reference trajectory is adapted to limit the interaction force and maintain it at a desired level, while feedforward force and impedance adaptation compensates for the interaction with the environment. An analysis of the interaction dynamics using Lyapunov theory yields the conditions for convergence of the closed-loop interaction mediated by this controller. Simulations exhibit adaptive properties similar to human motor adaptation. The implementation of this controller for typical interaction tasks including drilling, cutting, and haptic exploration shows that this controller can outperform conventional controllers in contact tooling.

Index Terms—Adaptive control, biological systems control, contact tasks, force control, iterative learning control, robot control.

Manuscript received July 19, 2017; revised November 16, 2017 and February 15, 2018; accepted April 2, 2018. This paper was recommended for publication by Associate Editor Y. Sun and Editor T. Murphey upon evaluation of the reviewers' comments. Y. Li, G. Ganesh, and N. Jarrassé contributed equally to the work. This work was supported by the European Commission Grants EU-FP7 VIATORS (ICT 231554) and CONTEST (ITN 317488), and EU-H2020 COGIMON (644727). (*Corresponding author: Yanan Li.*)

Y. Li was with the Department of Bioengineering, Imperial College of Science, Technology and Medicine, London SW7 2AZ, U.K. He is now with the Department of Engineering and Design, University of Sussex, Brighton, BN1 9RH, U.K. (e-mail: hit.li.yn@gmail.com).

G. Ganesh was with the Department of Bioengineering, Imperial College of Science, Technology and Medicine, London SW7 2AZ, U.K. He is now with the CNRS-AIST Joint Robotics Lab, Intelligent Systems and Research Institute, Tsukuba 305-0046, Japan (e-mail: gans_gs@hotmail.com).

N. Jarrassé was with the Department of Bioengineering, Imperial College of Science, Technology and Medicine, London SW7 2AZ, U.K. He is now with the CNRS, ISIR, UPMC Paris VI, Paris 75005, France (e-mail: jarrasse@isir.upmc.fr).

S. Haddadin was with the German Aerospace Center, Wessling 82234, Germany. He is now with the Institute of Automatic Control, Leibniz Universität Hannover, Hannover 30167, Germany (e-mail: sami.haddadin@irt.uni-hannover.de).

A. Albu-Schaeffer is with the Institute of Robotics and Mechatronics, German Aerospace Center, Wessling 82234, Germany (e-mail: Alin.Albu-Schaeffer@dlr.de).

E. Burdet is with the Department of Bioengineering, Imperial College of Science, Technology and Medicine, London SW7 2AZ, U.K. (e-mail: e.burdet@imperial.ac.uk).

Color versions of one or more of the figures in this paper are available online at <http://ieeexplore.ieee.org>.

Digital Object Identifier 10.1109/TRO.2018.2830405

I. INTRODUCTION

CONTACT tooling, such as drilling and carving, require dealing with the intrinsic instability resulting from the surface irregularities, unknown material properties, and motor noise. This control problem is exacerbated by the large forces often encountered during these tasks. Furthermore, contact tooling involves deformation or penetration of an object's surface, such that visual feedback is of little help to controllers. All these issues requisite the development of a suitable control strategy for regulating the movement and interaction force during contact tooling tasks.

Various interaction control techniques have been proposed by previous works. These include the *hybrid force-position control* [1] that decouples the force and position control in space, regulating position along the surface of an object and force normal to it. Good performance with this technique thus requires knowledge or good estimation of the surface geometry [2]. For instance, in [2] and [3], the surface geometry is estimated from the interaction force and position information. By regulating the relationship between the environment deformation and the force response, *impedance control* [4] can deal with environments that are not precisely known. However, controllers with fixed impedance do not *a priori* consider the instability arising from tool use, nor can they adapt to unknown surface conditions [5]–[7].

In contrast, humans can carry out unstable tooling tasks with ease, such as carving wooden pieces with knots, using a screwdriver, cutting with a knife, etc. This is arguably due to their capability to automatically compensate for the forces and instability in their environment [8]–[10]. We recently developed a computational model of this learning, which enabled us to simulate the characteristics of human motor learning in various stable and unstable dynamic environments [11], [12].

The dynamic properties of this learning controller were analyzed in [13], and used to demonstrate its capabilities for robot interaction control. This new robot behavior can adapt its end-point force and impedance to compensate for environmental disturbances. This controller increases robot force with the signed error relative to a given planned trajectory, increases the impedance when the unsigned error magnitude is large, and decreases impedance when the magnitude is small. While our previous controller in [13] can adapt to various environments, an obstacle on the robot reference trajectory can lead the force to increase and become very large.

How does the human sensorimotor control address this issue? Recent works that examined how humans interact with rigid objects [14], [15] found that the reference trajectory is deformed by the interaction with the object's surface, which limits and regulates the interaction force. We introduced in [16] a model of the concurrent adaptation of impedance, force, and trajectory characterizing the human adaptive behavior, and showed in simulation how it could predict human motor adaptation in various conditions. The extended nonlinear adaptive controller implementing this model adapts impedance and force, and guarantees the interaction stability by compensating for the disturbance from the environment, as is analyzed in the present paper. The interaction force is continuously estimated and used to adapt the reference trajectory so that the actual interaction force can be maintained at a desired level.

The model of human motor adaptation in [16] can be analyzed using Lyapunov theory, and used as a novel iterative learning controller (ILC) for robots. Specifically, we show in the present manuscript how the coupling between force/impedance adaptation and trajectory adaptation can be resolved. Simulations are used to study and exhibit the adaptation features. Implementations on DLR's 7-degree-of-freedom light weight robot (LWR) [17], [18] explore its use for representative tasks such as cutting, drilling, and haptic exploration similar to polishing, and demonstrate its versatility. Initial results were reported in [19] and [20], while extensive results are presented and analyzed in this paper¹.

While ILC has been investigated extensively [21]–[24], the present paper analyzes for the first time the coupling between impedance and/or force adaptation and trajectory adaptation. This coupling is interesting, since the updated impedance and/or force is used to adapt the reference trajectory and conversely the updated reference trajectory is also used to adapt the impedance/force. Section II and Appendix A extend the algorithm of [13] with trajectory adaptation to yield force control and adaptation of the shape and impedance of the environment. Section III interprets the theoretical results of Section II, Section IV illustrates the controller's functions through simulations, and Section V demonstrates its efficiency in implementations.

II. ADAPTATION OF FORCE, IMPEDANCE, AND PLANNED TRAJECTORY

In the following, we derive a general ILC for the interaction of a robot with an environment solely characterized by its stiffness and damping, using Lyapunov theory. The nomenclatures that will be used are summarized in Table I.

A. Controller Design

The dynamics of a n -DOF robot in the operational space are given by

$$M(q)\ddot{x} + C(q, \dot{q})\dot{x} + G(q) = u + f \quad (1)$$

where x is the position of the robot and q the vector of joint angle. u is the control input and f the interaction force applied

TABLE I
NOMENCLATURE

x	actual trajectory vector
q	joint angle vector
M, C, G	inertia, Coriolis and centrifugal, gravitational matrices
u	control input
f	interaction force from the environment
v	control component for compensation of robot's dynamics in free movements
w	control component for adaptation of force, stiffness and damping to interact with a novel environment
x_r	reference trajectory
e	tracking error
x_e	auxiliary trajectory
ε	auxiliary tracking error
Γ	linear control gain for free movements
L	positive-definite gain matrices
F^*, K_S^*, K_D^*, x_0^*	parameters of linear expansion of the environment mechanics: force, stiffness, damping and rest position
F, K_S, K_D	feedforward force, stiffness and damping of controller
Q_F, Q_K, Q_D, Q_r	learning rates for force, stiffness, damping and trajectory
β	decay rate of force, stiffness and damping
F_d	desired interaction force
J_c, J_e, J_r, J	costs of: impedance residual errors, tracking error, contact force error, and overall cost
T	movement trial or period
\bullet	$\bullet^* - \bullet$: difference of
$\Delta\bullet$	$\bullet(t+T) - \bullet(t)$: change of a factor during one period

by the environment. $M(q)$ denotes the inertia matrix, $C(q, \dot{q})\dot{x}$ the Coriolis and centrifugal forces, and $G(q)$ the gravitational force, which can be identified using, e.g., nonlinear adaptive control [25].

The control input u is separated in two parts

$$u = v + w. \quad (2)$$

In this equation, v is designed using a feedback linearization approach to track the *reference trajectory* x_r by compensating for the robot's dynamics, i.e.,

$$v = M(q)\ddot{x}_e + C(q, \dot{q})\dot{x}_e + G(q) - \Gamma\varepsilon \quad (3)$$

where

$$\dot{x}_e = \dot{x}_r - \alpha e, \quad e \equiv x - x_r, \quad \alpha > 0. \quad (4)$$

\dot{x}_e is an auxiliary variable and e is the tracking error. Γ is a symmetric positive-definite matrix having minimal eigenvalue $\lambda_{\min}(\Gamma) \geq \lambda_\Gamma > 0$ and ε is the sliding error

$$\varepsilon \equiv \dot{e} + \alpha e. \quad (5)$$

w , the second part of the control input u , is to adapt impedance and force in order to compensate for the unknown interaction dynamics with the environment, as will be described in this paragraph. Assuming that the environment can be characterized (locally) by its viscoelasticity, the interaction force can be expanded as

$$f = F_0^* + K_S^*(x - x_0^*) + K_D^*\dot{x} \quad (6)$$

where $F_0^*(t)$, $K_S^*(t)$, and $K_D^*(t)$ are force, stiffness, and damping experienced during interaction with the environment,

¹A video illustrating the experiments can be found at <https://www.youtube.com/watch?v=UZFL6oTHQBg> or on last author's website.

respectively, $x_0^*(t)$ is the rest position of the environment viscoelasticity. We use (6) to describe a general environment, which can be either passive with the force component $F_0^* = 0$ or active, such as a human arm or another robot. In this paper, we consider that the environment parameters are unknown but periodic with T

$$\begin{aligned} F_0^*(t+T) &\equiv F_0^*(t), \quad K_S^*(t+T) \equiv K_S^*(t), \\ K_D^*(t+T) &\equiv K_D^*(t), \quad x_0^*(t+T) \equiv x_0^*(t). \end{aligned} \quad (7)$$

The periodicity of the environment parameters is a realistic assumption for a repeatable interaction task, e.g., the surface exploration presented in the simulation of Section IV. In this example, the properties of the environment surface are the same for every session, so they are periodic along the time axis. In many applications, the environment parameters are constant thus also periodic. To simplify the analysis, we rewrite the interaction force of (6) as

$$f \equiv F^* + K_S^* x + K_D^* \dot{x} \quad (8)$$

with $F^* \equiv F_0^* - K_S^* x_0^*$ the feedforward force component of the environment. w in (2) is then defined as

$$w = -F - K_S x - K_D \dot{x} \quad (9)$$

where F , K_S , and K_D are feedforward force, stiffness, and damping components in the control input. As explained in the next paragraph, the contact stability is ensured through adapting F , K_S , K_D to match the environment's values F^* , K_S^* , K_D^* .

B. Force and Impedance Adaptation

By substituting the control input u into (1), the closed-loop system dynamics are described by

$$\begin{aligned} M(q) \dot{\varepsilon} + C(q, \dot{q}) \varepsilon + \Gamma \varepsilon &= \tilde{F} + \tilde{K}_S x + \tilde{K}_D \dot{x}, \\ \tilde{F} &\equiv F^* - F, \quad \tilde{K}_S \equiv K_S^* - K_S, \quad \tilde{K}_D \equiv K_D^* - K_D. \end{aligned} \quad (10)$$

In this equation, we see that the feedforward force F , stiffness K_S and damping K_D ensure contact stability by compensating for the interaction dynamics. Therefore, the objective of force and impedance adaptation is to minimize these residual errors. This can be carried out through minimizing the cost function

$$\begin{aligned} J_c(t) &\equiv \frac{1}{2} \int_{t-T}^t \tilde{F}^T Q_F^{-1} \tilde{F} + \text{vec}^T(\tilde{K}_S) Q_S^{-1} \text{vec}(\tilde{K}_S) \\ &\quad + \text{vec}^T(\tilde{K}_D) Q_D^{-1} \text{vec}(\tilde{K}_D) d\tau \end{aligned} \quad (11)$$

where Q_F , Q_S , and Q_D are symmetric positive-definite matrices, and $\text{vec}(\cdot)$ stands for the column vectorization operation. This objective is achieved through the following update laws:

$$\begin{aligned} \Delta F(t) &\equiv F(t) - F(t-T) = Q_F[\varepsilon(t) - \beta(t)F(t)] \quad (12) \\ \Delta K_S(t) &\equiv K_S(t) - K_S(t-T) \\ &= Q_S[\varepsilon(t)x(t)^T - \beta(t)K_S(t)] \\ \Delta K_D(t) &\equiv K_D(t) - K_D(t-T) \\ &= Q_D[\varepsilon \dot{x}(t)^T - \beta(t)K_D(t)] \end{aligned}$$

where F , K_S , and K_D are initialized as zero matrices/vectors with proper dimensions when their arguments are within $[0, T)$, and β is a decay factor. Concurrent adaptation of force and impedance in (12) corresponds to the computational model of human motor adaptation of [11]–[13].

Now that we have dealt with the interaction dynamics, trajectory tracking control can be obtained by minimizing the cost function

$$J_e(t) \equiv \frac{1}{2} \varepsilon(t)^T M(q) \varepsilon(t). \quad (13)$$

Consequently, we use a combined cost function

$$J \equiv J_c + J_e \quad (14)$$

that yields concurrent minimization of tracking error and residual impedance errors to adapt force and mechanical impedance during movement.

C. Trajectory Adaptation

The investigation of adaptation to stiff and compliant environments of [14] has shown that humans tend to apply a constant force on the surface, resulting in a different trajectory adaptation strategy depending on the surface stiffness. To model this behavior, we assume that the trajectory is adapted to maintain a desired contact force F_d with the environment's surface. In particular, assuming that there exists a desired trajectory x_d yielding F_d , i.e., from (6)

$$\begin{aligned} F_d &= F_0^* + K_S^*(x_d - x_0^*) + K_D^* \dot{x}_d \\ &= F^* + K_S^* x_d + K_D^* \dot{x}_d, \end{aligned} \quad (15)$$

we propose to adapt the reference x_r in order to track x_d . However, x_d is unknown, because the parameters F^* , K_S^* , and K_D^* in the interaction force are unknown. Nevertheless, we know that x_d is periodic with T , as F^* , K_S^* , and K_D^* are periodic with T and we also set F_d to be periodic with T .

In the following, we develop an update law to learn the desired trajectory x_d . First, we define

$$\xi_d \equiv K_S^* x_d + K_D^* \dot{x}_d, \quad \xi_r \equiv K_S x_r + K_D \dot{x}_r. \quad (16)$$

Then, we develop the following update law:

$$\Delta \xi_r(t) \equiv \xi_r(t) - \xi_r(t-T) \equiv L^{-T} Q_r [F_d(t) - F(t) - \xi_r(t)] \quad (17)$$

where Q_r and L are positive-definite constant gain matrices. This update law is developed to minimize the error between the desired force F_d and control force $-w = F + \xi_r$ as detailed in Appendix A. To consider the coupling of adaptation of force and impedance and trajectory adaptation, we modify the adaptation of feedforward force (12) to

$$\Delta F(t) = Q_F[\varepsilon(t) - \beta(t)F(t) + Q_r^T \Delta \xi_r(t)]. \quad (18)$$

Then, we obtain the update law for trajectory adaptation

$$\Delta x_r \equiv x_r(t) - x_r(t-T) \quad (19)$$

by solving

$$\Delta \xi_r = K_S \Delta x_r + K_D \Delta \dot{x}_r + \Delta K_S x_r + \Delta K_D \dot{x}_r \quad (20)$$

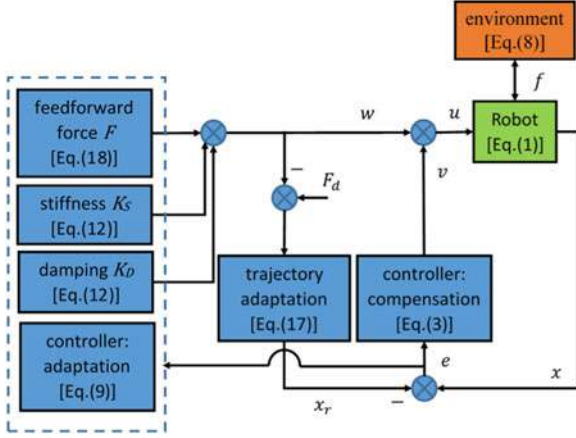


Fig. 1. Block diagram of proposed controller for dynamic interaction with, and adaptation to, unknown environments. The controller has three components: the dotted block represents the component to learn feedforward force and impedance in order to compensate for the interaction force from the environment; the trajectory adaptation component is to maintain a desired interaction force; and the compensation component compensates for the robot dynamics.

using $\Delta\xi_r(t)$ from (17), and $\Delta K_S, \Delta K_D$ from (12).

With (12), (17), and (18), we now have an algorithm able to adapt force, impedance, and trajectory in various dynamic environments. This is carried out by minimizing the overall cost $J \equiv J_c + J_e + J_r$ where

$$J_r \equiv \frac{1}{2} \int_{t-T}^t (\xi_r - \xi_d)^T Q_r^T (\xi_r - \xi_d) d\tau. \quad (21)$$

The result of this minimization is summarized in the following theorem.

Theorem 1: Considering the robot dynamics (1) and the interaction force model (8), the controller (2) with the update laws for stiffness and damping (12), feedforward force (18), and reference trajectory (17) will guarantee that the trajectory error $\Delta\xi_r$ and tracking error ε are bounded and satisfy

$$\begin{aligned} & \lambda_\Gamma \|\varepsilon\|^2 + \lambda_L \|\Delta\xi_r\|^2 \\ & \leq \frac{\beta}{2} (\|F^*\|^2 + \|\text{vec}(K_S^*)\|^2 + \|\text{vec}(K_D^*)\|^2) \end{aligned} \quad (22)$$

for $t \rightarrow \infty$, where λ_Γ and λ_L are the minimal eigenvalues of Γ and L , respectively. It follows that $\Delta\xi_r$ and ε can be made arbitrarily small by choosing sufficiently large λ_Γ and λ_L . Moreover, $\Delta\xi_r$ and ε will converge to zero for $\beta \equiv 0$.

A proof of Theorem 1 is given in Appendix A, which is based on the Lyapunov theory. The structure of the novel controller is illustrated in Fig. 1.

III. INTERPRETATION OF THEOREM 1

A. Parameters Convergence

To simplify the interpretation of Theorem 1, let us loosely state that for $t \rightarrow \infty$, $\Delta\xi_r = \varepsilon = 0$ (thus $\dot{\varepsilon} = 0$ if $\lim_{t \rightarrow \infty} \dot{\varepsilon}$ exists). With (17), we obtain $F_d = F + \xi_r$. According to the definitions of w in (9) and ξ_r in (16), we have $F + \xi_r = -w$ thus

$$F_d = -w. \quad (23)$$

On the other hand, the right-hand side of (10) is zero. According to the definitions of f in (8) and w in (9), we have

$$-w = f. \quad (24)$$

It follows $f = F_d$, which indicates that the desired interaction force F_d is maintained between the robot and the environment. According to the definitions of f and F_d in (8) and (15), respectively, we thus have

$$K_S^* x_d + K_D^* \dot{x}_d = K_S^* x + K_D^* \dot{x} \quad (25)$$

which leads to $x \rightarrow x_d$ if K_S^* and K_D^* are both positive definite.

However, note that the analysis of Appendix A does not show that F , K_S , and K_D converge to the respective values F^* , K_S^* , and K_D^* of the environment. This can be seen from (10): $\tilde{F} + \tilde{K}_S x + \tilde{K}_D \dot{x} = 0$ does not imply that \tilde{F} , \tilde{K}_S , and \tilde{K}_D become negligible. In order to achieve the convergence of F , \tilde{K}_S , and \tilde{K}_D to zero, the signals x and \dot{x} need to satisfy the condition of persistent excitation (PE) as in traditional adaptive control [26]. This will be illustrated in Section IV.

In summary, the proposed controller ensures that the interaction force f follows the desired force F_d and that the reference trajectory x_r follows x_d , the trajectory which yields F_d due to the physical properties of the environment. The controller parameters F , K_S , and K_D can track F^* , K_S^* , and K_D^* , respectively, if the signals x and \dot{x} are persistently exciting.

B. Important Special Cases

If no force is exerted on the environment: $f = 0$, the controller component $w = 0$ from (24). According to the definitions of w in (9) and ξ_r in (16), we have $F + \xi_r = -w = 0$. Therefore, if we choose $F_d = 0$, according to the update law (17), the reference trajectory will not adapt, as expected.

Another important case is when the feedforward force $F_0^* = 0$, damping $K_D^* = 0$, and stiffness $K_S^* \neq 0$, then (8) yields $x = x_0^*$ if we choose $F_d = 0$ since $f = F_d$. This indicates that the actual position follows the rest position of the environment, i.e., its surface.

If we neglect the damping component in the interaction force f of (8), the trajectory adaptation described by (17) and (20) can be simplified to

$$\Delta x_r = L^{-T} Q_r (F_d - F - K_S x_r). \quad (26)$$

Correspondingly, the update laws for force and impedance in (12) need to be modified as

$$\begin{aligned} \Delta F & \equiv Q_F (\varepsilon - \beta F + Q_r^T \Delta x_r), \\ \Delta K_S & \equiv Q_S (\varepsilon x^T - \beta K_S + x_r^T Q_r^T \Delta x_r) \end{aligned} \quad (27)$$

in order to obtain results similar to those described in Theorem 1. The interaction dynamics analysis, similar to the case with damping, is detailed in Appendix B.

C. Implicit and Explicit Force Sensing

In contrast to traditional methods for surface following where the force feedback is used to regulate the interaction force, e.g., [27], force sensing is not required in the above framework. In

particular, force and impedance adaptation [(12) and (18)] is used to compensate for the interaction force from the environment. During this process, the unknown actual interaction force is estimated when the tracking error ε goes to zero, i.e., (24). Using this estimated interaction force, a desired force in (15) can then be rendered by adaptation of the reference trajectory x_r [(17) and (20)].

If the robot system is equipped with a force sensor, force feedback can replace the force and impedance adaptation. In this way, trajectory adaptation will not depend on the force estimation process and can in principle happen faster. However, the potential advantages of a force sensor depend on the quality of its signal, its cost, and the difficulty of its installation and use.

IV. SIMULATIONS

We will now illustrate how the learning controller of previous section functions, by simulating the human motor adaptation in a representative interaction task [15]. This study observed the adaptation of force and trajectory in humans during contact with a rigid or compliant environment. Similarly, we simulated the adaptation of the reference trajectory occurring when one is required to push against environments of various stiffness. In this simulation, the desired force in forward direction is specified as

$$F_d = \begin{cases} -5[1 - \cos(\pi t)]N, & 0 \leq t \leq 1s; \\ -10N, & \text{otherwise.} \end{cases} \quad (28)$$

The interaction force of (8) is computed as

$$f = F^* + K_S^* y \quad (29)$$

corresponding to the rest position 0. The rigid environment is characterized by $F^* = -4N$ and $K_S^* = -1000 N/m$ and the compliant environment by $F^* = -3N$ and $K_S^* = -300 N/m$. The environment is rigid for the first 200 trials $j = 1 \dots 200$ and compliant for another 200 trials $j = 201 \dots 400$. The control and learning parameters used for simulation are $\alpha = 10$, $\Gamma = 200$, $\beta = 0$, $Q_S = 6 \times 10^4$, $Q_F = 3.6$, $Q_r = 0.02$.

Simulation results are shown in Fig. 2(a). The left column/panels exhibit that the desired force is achieved in the case of a rigid environment. The middle panels illustrate that when the environment suddenly becomes compliant, the desired force cannot be reached because of the trajectory control component. However, the trajectory iteratively moves forward and the interaction force increases. After learning, the reference trajectory has adapted to penetrate the environment surface and the desired interaction force is achieved again. Note that while the same desired force is achieved in the rigid environment, the reference trajectory changes with the different environments. The right panels illustrate the “after-effects” of the learning: when the environment becomes rigid again, the interaction force surpasses the desired force.

These results correspond to the behavior observed in human experiments [16]. Note the adaptation of force, impedance, and trajectory involved in the evolution: the reference trajectory adapts to achieve the desired force, while feedforward force and impedance adapt to track the updated reference trajectory.

However, in Fig. 2(a), the updated feedforward force and impedance do not converge to the values of the environment. This is due to the redundancy between the feedforward force and impedance as explained in Section III-A. While the combination of the feedforward force and impedance guarantees compensation for the interaction dynamics, it is not set to identify each component’s contribution.

The identification of the environment’s parameters can be addressed by introducing a PE signal yielding sufficiently rich information of the system. We illustrate this by adding a random binary excitation to the system as exhibited in Fig. 2(b). It can be seen that the identified interaction force and position values are similar to those in Fig. 2(a), but in this case the updated feedforward force and impedance converge to the environment’s values. The results in Fig. 2(a) and (b) also illustrate the meaning of redundancy between the feedforward force and impedance, as different values of feedforward force and impedance lead to the same interaction force and position. In practice, noise leading to the environment identification could stem from a rough surface along which the robot is moving [see Fig. 2(b)], while sliding on a smooth surface would lead to results similar to that in Fig. 2(a).

These results, together with the results of [16], show that the model of Section II predicts the adaptation of force, impedance, and trajectory observed when humans interact with various stable, unstable, stiff, and compliant environments [8], [11], [14], [15], [28], [29].

To illustrate the difference of the new controller relative to the adaptive controller of [13], Fig. 3 presents a simulation of polishing along (the x -axis of) a curved surface with both of these controllers. As shown in Fig. 3(a), as the controller of [13] tries to track the original reference trajectory (which is set as a straight line along the x -axis), this leads to a large contact force of around 20 N, which is undesirable. In contrast, Fig. 3(b) shows that with the new controller the robot’s trajectory comes close to the surface with learning (see “150th trial”), by tracking the updated reference trajectory, while the contact force tends to the desired force of about 1 N. Therefore, the new adaptive controller is extending the controller of [13]. It is able to successfully perform tasks requiring contact with rigid surfaces of unknown shape, and to identify the geometry and impedance properties of the surface it is interacting with.

V. ROBOTIC VALIDATION

The proposed controller was implemented on the DLR LWR shown in Fig. 4 [17], [18] and tested in various experiments. Four tasks were carried out: adaptation to a rigid surface, cutting, drilling, and haptic exploration, which are described in this section.

A. Adaptive Interaction With a Rigid Surface

To illustrate the trajectory adaptation to a rigid environment, one axis of the robot was programmed to repeat a movement of 0.7 radian amplitude following a smooth fifth-order polynomial reference, with zero start and end velocity and acceleration as shown in Fig. 5. After the robot converged on the reference trajectory (dashed blue trace), it was presented with a virtual

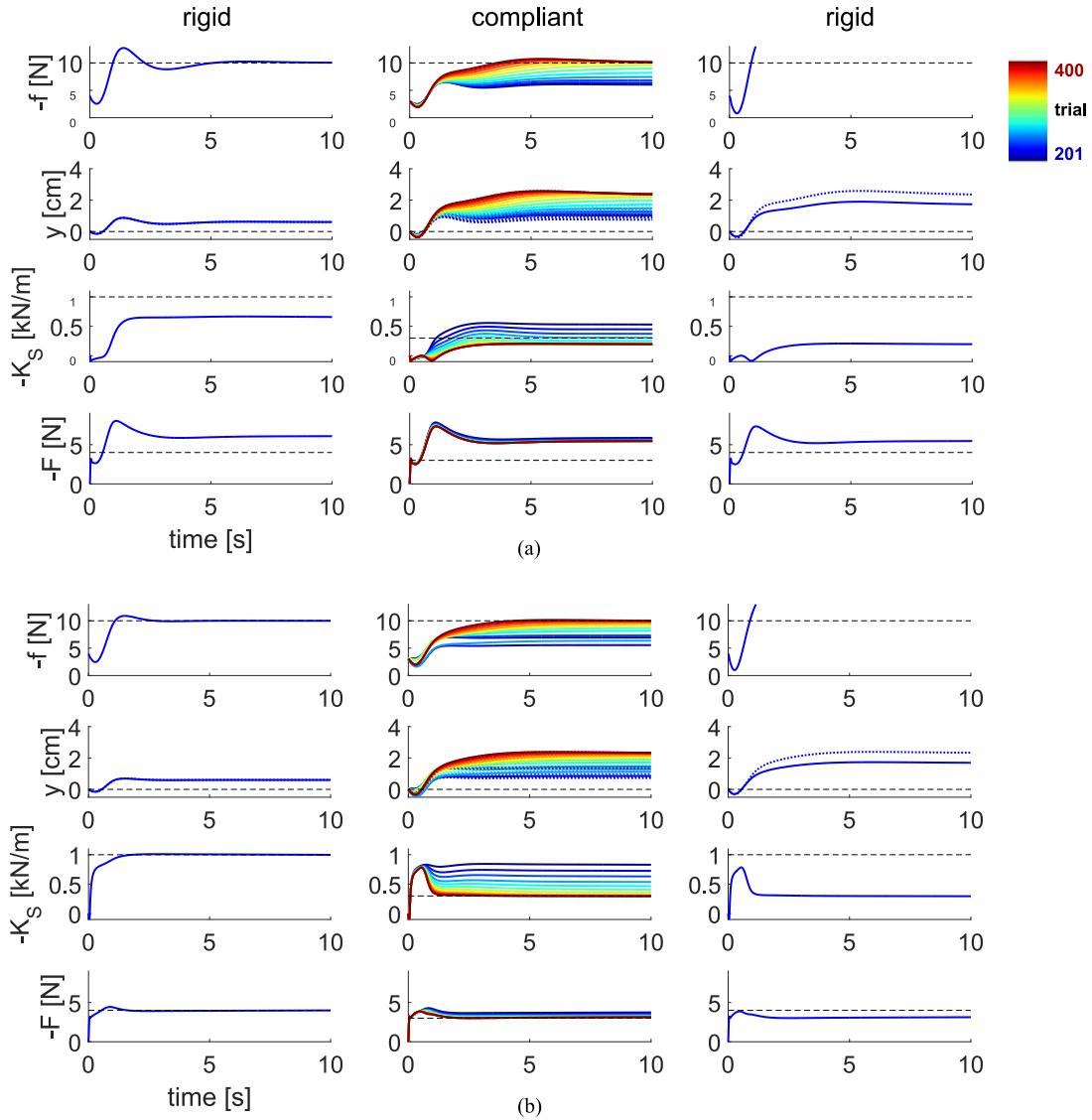


Fig. 2. Concurrent adaption of force, impedance, and trajectory (a) without noise and (b) with noise satisfying PE. From top to bottom: interaction force, actual trajectory (solid) and updated reference trajectory (dotted), updated stiffness, and updated feedforward force. From left to right: after learning in a rigid environment, in a compliant environment (plotted from blue to red in every 16 trials), and exposition to a rigid environment after learning in the compliant environment.

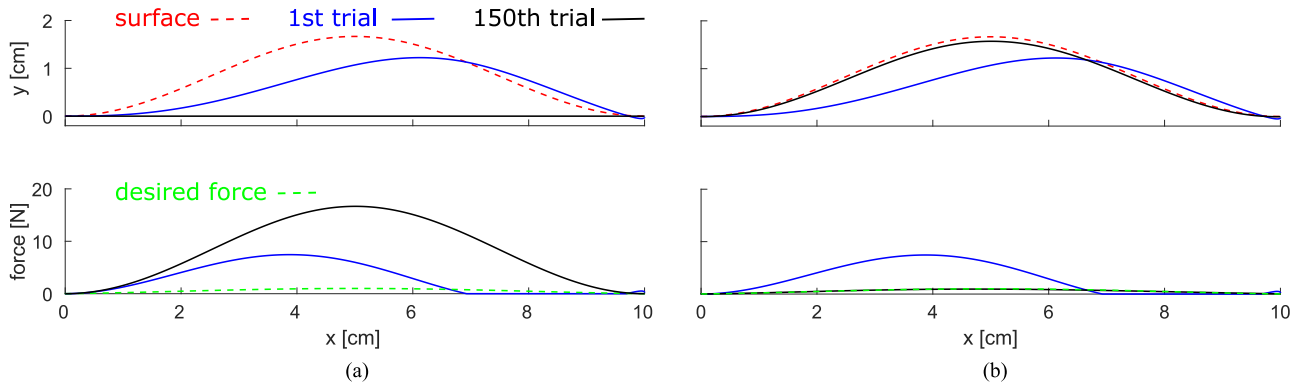


Fig. 3. Simulation of haptic exploration of a surface of unknown shape and mechanical properties along x -axis (a) with the controller of [13] and (b) with the new controller. The top panels show the robot's trajectory and the bottom panels the contact force. The new controller avoids large interaction force and enables regulation of the force, while identifying the interaction surface geometry.



Fig. 4. Setup of experiments described in Section V with the DLR LWR, the Dremel drill attached to the robot end-effector in the zoomed end-effector and the scalpel in the main panel.

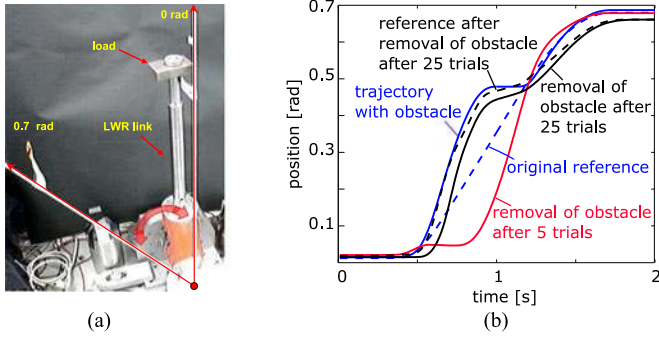


Fig. 5. Adaptation to a rigid surface. (a) 1-DOF robot. (b) Actual and reference trajectories.

obstacle in velocity space (blue trace) that prevented it from following the reference. This obstacle was generated by disconnecting the proposed controller output to the motor, and instead moving the robot along the obstacle using a high-gain PD controller, while the proposed controller was still active in the background. This simulated a situation where the controller was unable to generate sufficient motor output to overcome the obstacle.

When the obstacle was suddenly removed in the fifth adaptation trial, the robot movement was found to mirror the obstacle (red trace), as the robot initially tried to increase the torque to counter the obstacle. The obstacle was then reintroduced from the sixth trial onwards. When the obstacle was removed again in the 25th trial, the actual trajectory (black trace) and reference trajectory (dashed black trace) can be clearly seen to have adapted to the shape of the obstacle. The robot movement no longer mirrored the obstacle, i.e., it has learned not to apply a too large force in order to counter the obstacle, but instead has adapted its reference trajectory. The actual trajectory (black trace) can be seen to lie to the right-hand side of the plan (dashed black trace), indicating that the robot still did apply some contact force onto the obstacle after 25 trials. This behavior is similar to the adaptation observed in humans [14] as was analyzed in [16].

B. Cutting Experiment

Several experiments were then carried out to test adaptation of impedance and force during the interaction with unknown environments. For this purpose, a cutter or a drill was mounted on the LWR as shown in Fig. 4. Different from the previous simulation and the first experiment, in the next experiments iteration was in time rather than by repeating a trajectory. In this case, the LWR moved at low speed so that adaptation could catch the environment characteristics along the trajectory. The controller was programed to tune the adaptation gains differently along each axis of the end-effector frame $\{e_x, e_y, e_z\}$. A fixed high stiffness (2000 N/m) was maintained at the robot end effector in the $\{y \equiv 0\}$ plane, while the adaptive controller was used in the x - and z -directions. Stiffness saturation was set at 2000 N/m in all directions during the experiments. The same set of adaptation gains of $\beta = 0.01$, $Q_F = 5$, $Q_S = 120$, and $Q_r = 0.01$ was used during all the experiments in order to test the versatility of the adaptive controller in dealing with different tasks and environments without any manual tuning of the learning parameters. Q_r was set as zero in the cutting and drilling experiments.

We performed two cutting experiments using a scalpel that was fixed on the LWR end effector using a customized tool holder. The scalpel blade was maintained at a 65° angle to the surface. We used a heterogeneous test object in the first experiment that was made of a 2-mm balsa wood layer covered by a 2 mm layer of materials with different mechanical properties: balsa wood, plastic honeycomb panel, and brown corrugated cardboard. As can be seen in Fig. 6(b), the stiffness and feed-forward force were automatically adapted during the task to the specific material; stiffness increased due to the vibrations generated during the crossing of the carton and honeycomb sections and decreased during the crossing of the balsa wood section. On the other hand, the feedforward force increased during the crossing of the balsa wood section, because the wood is dense and generates a constant resistance to cutting.

The second cutting experiment was performed on a 3-cm thick expanded styrofoam board (made of 4 mm polystyrene balls agglomerated together, but with a smooth surface). The top surface of the board was painted in black to illustrate the damage done to the surface by the scalpel. Due to the material properties of styrofoam, it tends to stick to the blade and tear when the depth is too large for a given speed. We first determined a constant “depth/velocity” pair for our blade that leads to material tear (due to stick-slip) during cutting. Cutting was then carried out with this “depth/velocity” pair, first using a fixed high impedance (1500 N/m), then with the proposed adaptive controller starting from the same 1500 N/m stiffness value. As it can be seen in Fig. 6(c), our adaptive controller avoided the tearing phenomenon generated by the specific set of parameters (e.g., blade angle, velocity, and depth) though lowering the robot stiffness.

C. Drilling

We then compared drilling of a heterogeneous material using a fixed impedance (1500 N/m), and with adaptation using the

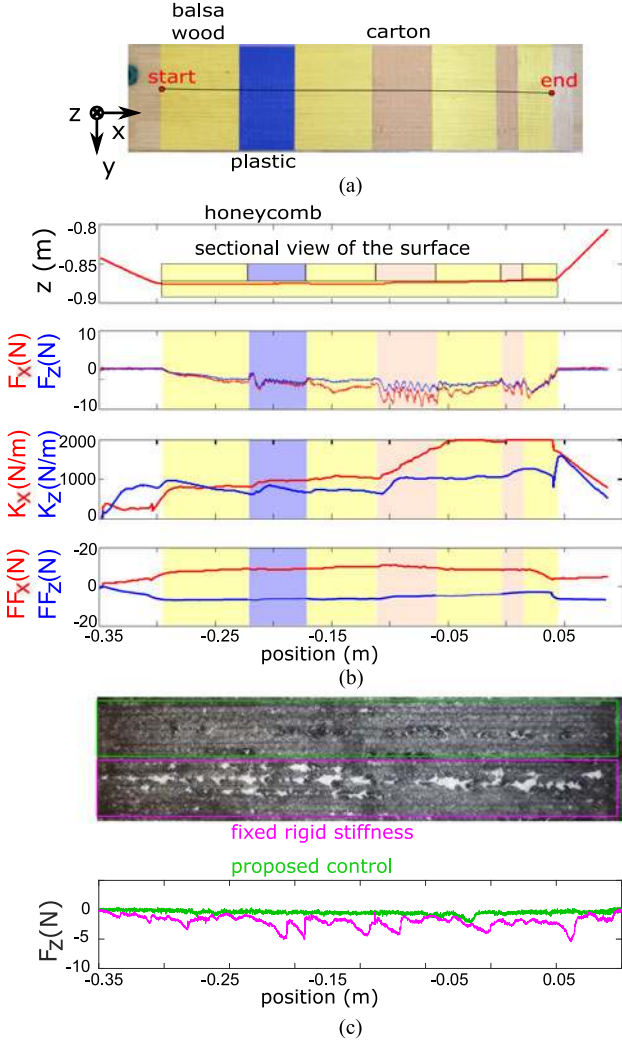


Fig. 6. Cutting through different materials. (a) View of the surface assembled with different materials (balsa wood, cardboard, and honeycomb plastic). (b) From top to bottom: blade trajectory across the section of the surface in the vertical plane; variations of the forces F_x and F_z along x - and z -directions, recorded by the 6-DOF force/torque sensor mounted between the robot and the scalpel; stiffness (K_x and K_z) and feedforward force (FF_x and FF_z) adaptation during the cutting task. (c) Visual results of cutting expanded styrofoam with/without biomimetic adaptation and associated force profile (along the cutting direction x).

proposed controller. Drilling was tested using a Dremel hand drill attached to the end-effector (through the force/torque sensor) at approximately 18 cm from the end-effector main axis. The force/torque sensor was used for the purpose of recording but not used in the proposed controller. The 3.2-mm diameter drill had to penetrate a heterogeneous block of material made of balsa wood layers (easy to drill) and some dense carton layers (requiring larger forces for drilling). As can be seen in Fig. 7, our controller was able to perform the task with results similar to the rigid impedance controller. However, at certain drilling speeds, the rigid impedance controller exhibited a “resonance” phenomenon [see Fig. 7(b)] that generated large vibrations in the horizontal plane (whose amplitude was proportional to the penetration of the drill bit), and consequently poorer quality of the drilled hole [larger variations in the diameter of the hole,

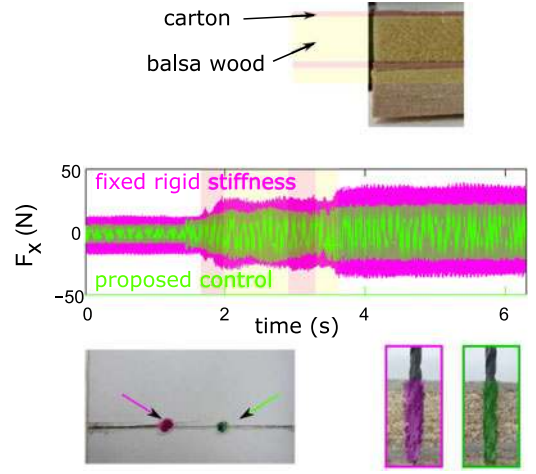


Fig. 7. Drilling heterogeneous material. (a) Section of the block. (b) Comparison of vibrations level in the horizontal plane transmitted to the robot structure (read on the force sensor) when using a driller speed generating “resonance,” without (red) and with (green) stiffness adaptation. (c) Adapting impedance reduced the hole carried out by the drill.

as seen in the bottom of Fig. 7(c)). The proposed controller attenuated these vibrations, resulting in a hole with a diameter closer to the real drill bit diameter.

D. Haptic Identification

To test concurrent adaptation of force, impedance, and trajectory, we implemented a haptic exploration experiment. The robot was required to traverse various surface profiles on a test surface while maintaining a constant contact force, a task that is similar to the polishing of an unknown surface. However, we designed the task to test the ability of the new controller to “skim” a surface with minimum force. We purposely used a very low desired interaction force level of 0.05 N and a soft foam surface so as to be able to visually check whether the robot would push and deform this surface.²

The test surface was developed on a wooden plank sized 85×95 cm. Various profiles, including convex bumps, concave troughs, and cylindrical obstacles, were created on this surface by fixing metal and plastic objects [see Fig. 8(a)]. A 3-cm thick layer of packing foam was then overlaid on the surface. The test surface included a high friction pad created using twisted nylon ropes and a hole in the surface. The test surface was placed on a table under the robot, which was equipped with a 12-cm long aluminium finger at the end-effector. The robot reference was set to scan the plane of the table over a range of 120 cm and with a constant speed of 0.1 m/s (except for the accelerations and de-accelerations in the movement limits). The reference was set in the task space and the trajectory was developed using the interpolator of the manipulator.

Fig. 8(b) shows the surface traced by the robot. Fig. 8(c) shows the tool-tip coordinates of the robot in the x - y plane of the table with the color gradient representing the z -coordinate (height above the table). Fig. 8(d) plots the endpoint stiffness of the robot as it performed the surface exploration while Fig. 8(e)

²See the video in <https://www.youtube.com/watch?v=UZFL6oTHQBg>.

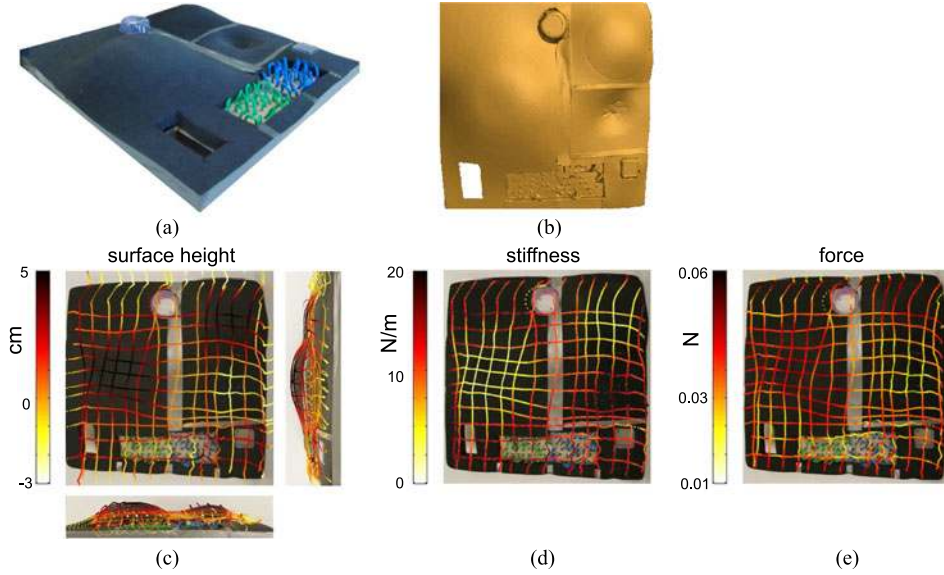


Fig. 8. Haptic exploration of a surface with unknown geometry and mechanics. From left to right: (a) Photo of the test surface that was used for the pilot experiment. (b) 3-D scan of the test surface. (c) Volume identified by the robot while scanning the surface along the line superimposed on top and two lateral views. (d) End point stiffness during exploration. (e) Nearly constant interaction force of about 0.05 N maintained on the surface.

shows the contact force along the vertical z -axis as measured from the end-point force/torque sensor (not used for control). We conducted an analysis of the force sensor inside the surface boundaries, which exhibit a force of 0.0338 N in average with a standard deviation of 0.0088 N. To show that this is not an offset on the force sensor, or noise, we compared this value to the one from outside the surface in the same experiment. The value from outside the surface (when there is no contact) is 0.0151 N in average with a standard deviation of 0.0109 N, which is statistically smaller than the one inside the surface boundaries ($p < 0.001$). Stiffness is maintained at a low value throughout the exploration and increases only in the edges of the surface and in the region with irregularities. The stiffness change thus indicates the texture properties of the surface.

VI. DISCUSSION

Many tasks with end-effector held tools are inherently unstable, require large contact forces, and are subject to disturbances due to the irregularities on the tooled surface. While robots have been conceived to address these challenges in specific and well-defined situations, humans routinely use tools in different tasks such as drilling, cutting, and polishing, adapting to various environments, despite large sensorimotor noise. In fact, human intelligence has been characterized by the skilful use of tools [30], and specific neural structures could be identified in humans [31] that correspond to force and impedance adaptations. While we do not pretend to match such manipulation intelligence, the controller analyzed in this paper exhibited a versatile interaction behavior, and was also shown to model human interaction properties in typical situations [16].

Our controller for contact tooling and haptic identification automatically adapts feedforward force, mechanical impedance, and trajectory to the environment dynamics in order to mini-

mize trajectory error and effort while applying a desired force. It compensates for the interaction force and instability to track the planned reference trajectory. During this process, the controller is able to estimate the interaction force with the unknown environment through adaptation of feedforward force and impedance. It extends the functionality of the controller introduced in [13], by automatically adapting its reference trajectory to comply with rigid environments, and to maintain a desired interaction force.

The proposed controller, developed based on the assumption of a linearized interaction force [(6)], can interact with a rigid environment or a compliant force field, or with humans. It can be used to automatically tune physical assistance in, e.g., a rehabilitation robot [32]. It does not require a force sensor as the force is estimated by the algorithm. Using a force sensor will however speed up the adaptation of feedforward force, stiffness, and trajectory, although this may depend on the quality of the force signal and on its noise.

The stability and convergence of this novel nonlinear adaptive controller have been rigorously analyzed using the Lyapunov theory. An implementation on the DLR 7-DOF LWR demonstrated its effectiveness and versatility in representative interaction tasks including cutting, drilling, and haptic exploration. With this controller, the robot constantly adapts its behavior to the environment, rather than rigidly trying to go through. Feedforward force adaptation is essential for tasks like cutting, where the material irregularities continuously modify the required cutting force. Impedance adaptation helps counter these variations, while maintaining minimum stiffness of the cutting tool. Trajectory adaptation enables maintenance of contact force during tasks like polishing and prevents the robot from applying very high forces in the presence of unforeseen obstacles.

Experimental results demonstrated superior performance of the novel adaptive controller relative to a fixed impedance controller: smoother interaction, reduced control effort, and automatic adaptation (avoiding tedious trial-and-error and fine tuning). Moreover, the properties of the unknown environment could be identified through adaptation during slow interaction movements yielding haptic exploration. As in any tooling task, our algorithm does require some basic parameter definition for each tooling operation such as cutting speed and depth of cut prescribed by tool manufacturer for a given tool-surface combination. However, it does not require any information or model of the surface irregularities, material, and shape of the tool surface.

The proposed controller can be applied to interact with environments that can be described by (6), characterized by periodic or constant parameters. If the environment parameters keep changing and the periodicity condition is not satisfied, e.g., when interacting with a human arm, the controller can still successfully adapt as long as the environment parameter changes are *slow*, but may fail otherwise. Larger controller learning rates (Q_F, Q_K, Q_D, Q_r) may enable it to adapt to fast changing environments, although too large learning rates may reduce the system robustness. On the other hand, improper choice of initial controller parameters may lead to task failure. For instance, during a surface polishing task, a controller with high initial stiffness can make the robot get stuck in rough stiff surface. The interesting meta learning issue of choosing the appropriate learning rates and initial parameters need to be investigated in further studies.

APPENDIX

A. Proof of Theorem 1

A Lyapunov-like analysis of the closed-loop learning control is carried out here in four steps. The first three steps consider the difference between two consecutive periods of the Lyapunov function candidates J_r (error of contact force), J_c (residual impedance errors), and J_e (tracking error), respectively. Step 4 then uses the results of the first three steps to examine the difference between two consecutive periods of the overall cost $J \equiv J_r + J_c + J_e$.

Step 1: Contact force error

Considering the definition of J_r in (21), we have

$$\begin{aligned} \Delta J_r(t) &\equiv J_r(t) - J_r(t-T) \\ &= \frac{1}{2} \int_{t-T}^t [\xi_r(\tau) - \xi_d(\tau)]^T Q_r^T [\xi_r(\tau) - \xi_d(\tau)] d\tau \\ &\quad - \frac{1}{2} \int_{t-T}^t [\xi_r(\tau) - \xi_d(\tau)]^T Q_r^T [\xi_r(\tau-T) - \xi_d(\tau-T)] d\tau \\ &\quad + \frac{1}{2} \int_{t-T}^t [\xi_r(\tau) - \xi_d(\tau)]^T Q_r^T [\xi_r(\tau-T) - \xi_d(\tau-T)] d\tau \\ &\quad - \frac{1}{2} \int_{t-T}^t [\xi_r(\tau-T) - \xi_d(\tau-T)]^T Q_r^T \times \\ &\quad [\xi_r(\tau-T) - \xi_d(\tau-T)] d\tau \end{aligned}$$

$$\begin{aligned} &= \frac{1}{2} \int_{t-T}^t [\xi_r(\tau) - \xi_d(\tau)]^T Q_r^T \Delta \xi_r(\tau) d\tau \\ &\quad + \frac{1}{2} \int_{t-T}^t [\xi_r(\tau-T) - \xi_d(\tau-T)]^T Q_r^T \Delta \xi_r(\tau) d\tau \\ &= \int_{t-T}^t [\xi_r - \xi_d - \frac{1}{2} \Delta \xi_r]^T Q_r^T \Delta \xi_r d\tau \quad (\text{as } \xi_d(t) = \xi_d(t-T)) \\ &\leq \int_{t-T}^t [Q_r(\xi_r(\tau) - \xi_d(\tau))]^T \Delta \xi_r(\tau) d\tau. \end{aligned} \quad (30)$$

According to (15) to (17), we rewrite this inequality as

$$\begin{aligned} \Delta J_r &\leq \int_{t-T}^t [Q_r(\xi_r - F_d + F + \tilde{F})]^T \Delta \xi_r d\tau \\ &= \int_{t-T}^t (-L^T \Delta \xi_r + Q_r \tilde{F})^T \Delta \xi_r d\tau. \end{aligned} \quad (31)$$

Step 2: Residual impedance error

Consider the difference between J_c of two consecutive periods

$$\begin{aligned} \Delta J_c &\equiv J_c - J_c(t-T) \\ &= \frac{1}{2} \int_{t-T}^t [(\tilde{F}^T Q_F^{-1} \tilde{F} - \tilde{F}^T(\tau-T) Q_F^{-1} \tilde{F}(\tau-T)) \\ &\quad + \text{tr}(\tilde{K}_S^T Q_S^{-1} \tilde{K}_S - \tilde{K}_S^T(\tau-T) Q_S^{-1} \tilde{K}_S(\tau-T)) \\ &\quad + (\tilde{K}_D^T Q_D^{-1} \tilde{K}_D - \tilde{K}_D^T(\tau-T) Q_D^{-1} \tilde{K}_D(\tau-T))] d\tau \end{aligned} \quad (32)$$

where $\text{tr}(\cdot)$ stands for the trace of a matrix. We compute

$$\begin{aligned} &\tilde{F}^T(\tau) Q_F^{-1} \tilde{F}(\tau) - \tilde{F}^T(\tau-T) Q_F^{-1} \tilde{F}(\tau-T) \\ &= [\tilde{F}^T(\tau) Q_F^{-1} \tilde{F}(\tau) - \tilde{F}^T(\tau) Q_F^{-1} \tilde{F}(\tau-T)] \\ &\quad + [\tilde{F}^T(\tau) Q_F^{-1} \tilde{F}(\tau-T) - \tilde{F}^T(\tau-T) Q_F^{-1} \tilde{F}(\tau-T)] \\ &= -\tilde{F}^T(\tau) Q_F^{-1} \Delta F(\tau) - \tilde{F}^T(\tau-T) Q_F^{-1} \Delta F(\tau) \\ &= -(2\tilde{F}^T(\tau) + \Delta F(\tau)) Q_F^{-1} \Delta F(\tau) \\ &\leq -2\tilde{F}^T(\tau) Q_F^{-1} \Delta F(\tau) \\ &= -2\tilde{F}^T(\tau) [\varepsilon(\tau) - \beta(\tau) F(\tau) + Q_r^T \Delta \xi_r(\tau)]. \end{aligned} \quad (33)$$

Similarly we have

$$\begin{aligned} &\text{tr}[\tilde{K}_S^T(\tau) Q_S^{-1} \tilde{K}_S(\tau) - \tilde{K}_S^T(\tau) Q_S^{-1} \tilde{K}_S(\tau-T)] \\ &\leq -2\text{tr}\{\tilde{K}_S^T(\tau) [\varepsilon(\tau) x^T(\tau) - \beta(\tau) K_S(\tau)]\} \\ &\quad \text{tr}[\tilde{K}_D^T(\tau) Q_D^{-1} \tilde{K}_D(\tau) - \tilde{K}_D^T(\tau-T) Q_D^{-1} \tilde{K}_D(\tau-T)] \\ &\leq -2\text{tr}[\tilde{K}_D^T(\tau) (\varepsilon(\tau) \dot{x}^T(\tau) - \beta(\tau) K_D(\tau))]. \end{aligned} \quad (34)$$

Substituting (33) and (34) into (32) and considering (31), we obtain

$$\begin{aligned} \Delta J_r + \Delta J_c &\leq \int_{t-T}^t -\Delta \xi_r^T L \Delta \xi_r - \tilde{F}^T(\varepsilon - \beta F) \\ &\quad - \text{tr}[\tilde{K}_S^T(\varepsilon x^T - \beta K_S)] - \text{tr}[\tilde{K}_D^T(\varepsilon \dot{x}^T - \beta K_D)] d\tau. \end{aligned} \quad (35)$$

Step 3: Tracking error

The rest of the derivations deals with the residual in above inequality, which is similar to that in [13]. For completeness, we outline this in the following. In particular, we consider the time derivative of J_e

$$\dot{J}_e = \varepsilon^T M \dot{\varepsilon} + \frac{1}{2} \varepsilon^T \dot{M} \varepsilon = \varepsilon^T M \dot{\varepsilon} + \varepsilon^T C \varepsilon \quad (36)$$

as [33]

$$z^T \dot{M} z \equiv 2z^T C z \quad \forall z. \quad (37)$$

Considering the closed-loop dynamics (10), above equation can be written as

$$\dot{J}_e(t) \equiv \varepsilon^T (\tilde{F}^T + \tilde{K}_S^T x + \tilde{K}_D^T \dot{x} - \Gamma \varepsilon). \quad (38)$$

Integrating \dot{J}_e from $t - T$ to t and considering (35), we obtain

$$\Delta J_e = \int_{t-T}^t -\varepsilon^T \Gamma \varepsilon + \tilde{F}^T \varepsilon + \text{tr}(\tilde{K}_S^T \varepsilon x^T) + \text{tr}(\tilde{K}_D^T \varepsilon \dot{x}^T) d\tau. \quad (39)$$

Step 4: Overall cost J

Considering (35) and (39), we can now calculate

$$\begin{aligned} \Delta J &= \Delta J_c + \Delta J_r + \Delta J_e \\ &\leq \int_{t-T}^t -\varepsilon^T \Gamma \varepsilon - \Delta \xi_r^T L \Delta \xi_r \\ &\quad + \beta [\tilde{F}^T F + \text{tr}(\tilde{K}_S^T K_S + \tilde{K}_D^T K_D)] d\tau \\ &= \int_{t-T}^t -\varepsilon^T \Gamma \varepsilon - \Delta \xi_r^T L \Delta \xi_r - \beta [\tilde{F}^T \tilde{F} \\ &\quad + \text{tr}(\tilde{K}_S^T \tilde{K}_S + \tilde{K}_D^T \tilde{K}_D)] \\ &\quad + \beta [\tilde{F}^T F^* + \text{tr}(\tilde{K}_S^T K_S^* + \tilde{K}_D^T K_D^*)] d\tau. \end{aligned} \quad (40)$$

According to (40), a sufficient condition for $\Delta J \leq 0$ is

$$\begin{aligned} &\lambda_\Gamma \|\varepsilon\|^2 + \lambda_L \|\Delta \xi_r\|^2 + \beta (\|\tilde{F}\|^2 + \|\text{vec}(\tilde{K}_S)\|^2 \\ &\quad + \|\text{vec}(\tilde{K}_D)\|^2) - \beta (\|\tilde{F}\| \|F^*\| + \|\text{vec}(\tilde{K}_S)\| \|\text{vec}(K_S^*)\| \\ &\quad + \|\text{vec}(\tilde{K}_D)\| \|\text{vec}(K_D^*)\|) \geq 0. \end{aligned} \quad (41)$$

Therefore, the following inequality is satisfied:

$$\begin{aligned} &\lambda_\Gamma \|\varepsilon\|^2 + \lambda_L \|\Delta \xi_r\|^2 + \frac{\beta}{2} (\|\tilde{F}\|^2 + \|\text{vec}(\tilde{K}_S)\|^2 \\ &\quad + \|\text{vec}(\tilde{K}_D)\|^2) \leq \frac{\beta}{2} (\|F^*\|^2 + \|\text{vec}(K_S^*)\|^2 + \|\text{vec}(K_D^*)\|^2). \end{aligned} \quad (42)$$

The above inequality can be proved by contradiction: assuming the above inequality is invalid yields $\Delta J < 0$ and thus J decreases iteratively. This indicates that $\|\varepsilon\|$, $\|\Delta \xi_r\|$, $\|\tilde{F}\|$, $\|\text{vec}(\tilde{K}_S)\|$ or $\|\text{vec}(\tilde{K}_D)\|$ (and thus the left-hand side of the above inequality) become even smaller, which contradicts the hypothesis.

From the above inequality, we obtain (22), which indicates that $\Delta \xi_r$ and ε can be made arbitrarily small by choosing sufficiently large λ_Γ and λ_L . Moreover, if we select $\beta \equiv 0$, $\Delta \xi_r$ and ε will converge to zero.

B. Stability Analysis When Neglecting Damping

Consider the cost function

$$J'_r \equiv \frac{1}{2} \int_{t-T}^t (x_r - x_d)^T K_S^{*T} Q_r^T (x_r - x_d) d\tau. \quad (43)$$

Following similar procedures to (30) and (31), we obtain

$$\Delta J'_r \leq \int_{t-T}^t [-L^T \Delta x_r + Q_r (\tilde{F} + \tilde{K}_S x_r)]^T \Delta x_r d\tau. \quad (44)$$

Considering further the cost function

$$J'_c \equiv \frac{1}{2} \int_{t-T}^t \tilde{F}^T Q_F^{-1} \tilde{F} + \text{vec}^T(\tilde{K}_S) Q_S^{-1} \text{vec}(\tilde{K}_S) d\tau \quad (45)$$

and following similar procedures from (32) to (35), we obtain

$$\begin{aligned} \Delta J'_r + \Delta J'_c &\leq \int_{t-T}^t -\Delta x_r^T L \Delta x_r - \tilde{F}^T (\varepsilon - \beta F) \\ &\quad - \text{tr}[\tilde{K}_S^T (\varepsilon x^T - \beta K_S)] d\tau. \end{aligned} \quad (46)$$

The rest is similar to the case with damping and thus omitted.

REFERENCES

- [1] O. Khatib, "A unified approach for motion and force control of robot manipulators: The operational space formulation," *IEEE J. Robot. Autom.*, vol. RA-3, no. 1, pp. 43–53, Feb. 1987.
- [2] K. Kiguchi and T. Fukuda, "Position/force control of robot manipulators for geometrically unknown objects using fuzzy neural networks," *IEEE Trans. Ind. Electron.*, vol. 47, no. 3, pp. 641–649, Jun. 2000.
- [3] Z.-W. Luo, K. Ito, and M. Yamakita, "Estimation of environment models using vector field and its application to robot's contact tasks," in *Proc. IEEE Int. Conf. Neural Netw.*, Nov. 1995, vol. 5, pp. 2546–2549.
- [4] N. Hogan, "Impedance control: An approach to manipulation," *Trans. ASME J. Dyn. Syst. Meas. Control*, vol. 107, no. 1, pp. 1–24, 1985.
- [5] D. Braun, M. Howard, and S. Vijayakumar, "Optimal variable stiffness control: Formulation and application to explosive movement tasks," *Auton. Robots*, vol. 33, no. 3, pp. 237–53, 2012.
- [6] A. Ajoudani, M. Gabbicini, N. Tsagarakis, and A. Bicchi, "Human-like impedance and minimum effort control for natural and efficient manipulation," in *Proc. IEEE Int. Conf. Robot. Autom.*, 2013, pp. 4499–4505.
- [7] M. Erden and A. Billard, "Robotic assistance by impedance compensation for hand movements while manual welding," *IEEE Trans. Cybern.*, vol. 46, no. 11, pp. 2459–72, Nov. 2016.
- [8] E. Burdet, R. Osu, D. Franklin, T. Milner, and M. Kawato, "The central nervous system stabilizes unstable dynamics by learning optimal impedance," *Nature*, vol. 414, no. 6862, pp. 446–449, 2001.
- [9] D. Franklin, R. Osu, E. Burdet, M. Kawato, and T. Milner, "Adaptation to stable and unstable dynamics achieved by combined impedance control and inverse dynamics model," *J. Neurophysiology*, vol. 90, no. 5, pp. 3270–3282, 2003.
- [10] D. Franklin, G. Liaw, T. Milner, R. Osu, E. Burdet, and M. Kawato, "Endpoint stiffness of the arm is directionally tuned to instability in the environment," *J. Neurosci.*, vol. 27, no. 29, pp. 7705–7716, 2007.
- [11] D. Franklin *et al.*, "CNS learns stable, accurate, and efficient movements using a simple algorithm," *J. Neurosci.*, vol. 28, no. 44, pp. 11165–11173, 2008.
- [12] K. Tee, D. Franklin, M. Kawato, T. Milner, and E. Burdet, "Concurrent adaptation of force and impedance in the redundant muscle system," *Biol. Cybern.*, vol. 102, no. 1, pp. 31–44, 2010.
- [13] C. Yang, G. Ganesh, S. Haddadin, S. Parusel, A. Albu-Schaeffer, and E. Burdet, "Human-like adaptation of force and impedance in stable and unstable interactions," *IEEE Trans. Robot.*, vol. 21, no. 5, pp. 918–30, Oct. 2011.
- [14] V. Chib, J. Patton, K. Lynch, and F. Mussa-Ivaldi, "Haptic identification of surfaces as fields of force," *J. Neurophysiology*, vol. 95, no. 2, pp. 1068–1077, 2005.

- [15] M. Casadio, A. Pressman, and S. Mussa-Ivaldi, "Learning to push and learning to move: The adaptive control of contact forces," *Frontiers Comput. Neurosci.*, vol. 9, no. 118, pp. 1–17, 2015.
- [16] Y. Li, N. Jarrassé, and E. Burdet, "Versatile interaction control and haptic identification in humans and robots," in *Geometric and Numerical Foundations of Movements*, J.-P. Laumond, N. Mansard, and J.-B. Lasserre, Eds., vol. 117. New York, NY USA: Springer, 2017, pp. 187–206.
- [17] A. Albu-Schäffer, C. Ott, and G. Hirzinger, "A unified passivity based control framework for position, torque and impedance control of flexible joint robots," *Int. J. Robot. Res.*, vol. 26, no. 1, pp. 23–39, 2007.
- [18] A. Albu-Schäffer *et al.*, "Soft robotics: From torque feedback controlled lightweight robots to intrinsically compliant systems," *IEEE Robot. Autom. Mag.*, vol. 15, no. 3, pp. 20–30, Jan. 2008.
- [19] G. Ganesh, A. Albu-Schaeffer, M. Haruno, M. Kawato, and E. Burdet, "Biomimetic motor behavior for simultaneous adaptation of force, impedance and trajectory in interaction tasks," in *Proc. IEEE Int. Conf. Robot. Autom.*, 2010, pp. 2705–2711.
- [20] G. Ganesh, N. Jarrassé, S. Haddadin, A. Albu-Schaeffer, and E. Burdet, "A versatile biomimetic controller for contact tooling and haptic exploration," in *Proc. IEEE Int. Conf. Robot. Autom.*, 2012, pp. 3329–3334.
- [21] S. Arimoto, S. Kawamura, and F. Miyazaki, "Bettering operation of robots by learning," *J. Field Robot.*, vol. 1, no. 2, pp. 123–140, 1984.
- [22] D. A. Bristow, M. Tharayil, and A. G. Alleyne, "A survey of iterative learning control," *IEEE Control Syst.*, vol. 26, no. 3, pp. 96–114, Jun. 2006.
- [23] Z. Bien and J.-X. Xu, *Iterative Learning Control: Analysis, Design, Integration and Applications*. New York, NY, USA: Springer, 2012.
- [24] K. L. Moore, *Iterative Learning Control for Deterministic Systems*. New York, NY, USA: Springer, 2012.
- [25] E. Burdet, A. Codourey, and L. Rey, "Experimental evaluation of nonlinear adaptive controllers," *IEEE Control Syst. Mag.*, vol. 18, no. 2, pp. 39–47, Apr. 1998.
- [26] K. Åström and B. Wittenmark, *Adaptive Control*. Reading, MA, USA: Addison-Wesley, 1995.
- [27] S. Jung, T. Hsia, and R. Bonitz, "Force tracking impedance control for robot manipulators with an unknown environment: theory, simulation, and experiment," *Int. J. Robot. Res.*, vol. 20, no. 9, pp. 765–774, 2001.
- [28] R. Shadmehr and F. Mussa-Ivaldi, "Adaptive representation of dynamics during learning of a motor task," *J. Neurosci.*, vol. 14, no. 5, pp. 3208–3224, 1994.
- [29] R. Osu, E. Burdet, D. Franklin, T. Milner, and M. Kawato, "Different mechanisms in adaptation to stable and unstable dynamics," *J. Neurophysiology*, vol. 90, no. 5, pp. 3255–3269, 2003.
- [30] K. Vaesen, "The cognitive bases of human tool use," *Behavioral Brain Sci.*, vol. 35, no. 4, pp. 203–218, 2012.
- [31] M. Haruno, G. Ganesh, E. Burdet, and M. Kawato, "Distinct neural correlates of reciprocal- and co-activation of muscles in dorsal and ventral premotor cortices," *J. Neurophysiology*, vol. 107, pp. 126–133, 2012.
- [32] N. Jarrassé, T. Charalambous, and E. Burdet, "A framework to describe, analyze and generate interactive motor behaviors," *PLoS ONE*, vol. 7, no. 11, 2012, Art. no. e49945.
- [33] C. de Wit, B. Siciliano, and G. Bastin, *Theory of Robot Control*. New York, NY, USA: Springer, 1996.



Yanan Li (S'10–M'14) received the B.Eng. and M.Eng. degrees from the Harbin Institute of Technology, Harbin, China, in 2006 and 2008, respectively, and the Ph.D. degree from the National University of Singapore, Singapore, in 2013.

He is currently a Lecturer in control engineering with the Department of Engineering and Design, University of Sussex, Sussex, U.K. From 2015 to 2017, he was a Research Associate with the Department of Bioengineering, Imperial College London, London, U.K. From 2013 to 2015, he was a Research Scientist with the Institute for Infocomm Research, Agency for Science, Technology and Research, Singapore. His general research interests include human–robot interaction, assistive robotics, human motor control, and control theory and applications.



Gowrishankar Ganesh (M'08) received the Bachelor's of Engineering (first-class, Hons.) degree from the Delhi College of Engineering, New Delhi, India, in 2002 and the Master's of Engineering degree from the National University of Singapore, Singapore, in 2005, both in mechanical engineering. He received the Ph.D. degree in bioengineering from Imperial College London, London, U.K., in 2010.

He was an Intern Researcher with the Computational Neuroscience Laboratories, Advanced Telecommunication Research (ATR), Kyoto, Japan, from 2004 to 2010. Following his Ph.D., he was with the National Institute of Information and Communications Technology as a Specialist Researcher until December 2013. Since January 2014, he has been a Senior Researcher with the Centre National de la Recherche Scientifique (CNRS), and is currently located at the CNRS-AIST Joint Robotics Lab, Tsukuba, Japan. He is a Visiting Researcher with the National Institute of Advanced Industrial Science and Technology, Centre for Information and Neural Networks, Osaka, Japan, ATR, and the Laboratoire d'Informatique, de Robotique et de Microélectronique de Montpellier, Montpellier, France. His research interests include human sensory-motor control and learning, robot control, social neuroscience, and robot–human interactions.



Nathanaël Jarrassé received the M.Sc. degree in industrial systems engineering from Arts et Métiers ParisTech, Paris, France, and the M.Sc. and the Ph.D. degrees in robotics from University Pierre and Marie Curie, Paris, France.

He has been a Postdoctoral Research Associate with the Human Robotics Group, Department of Bioengineering, Imperial College London, and is now a Tenured Researcher for the National Center for Scientific Research, ISIR, Sorbonne Université, Paris, France. His research focuses on physical human–

robot interaction for medical applications, and aims at developing robotic interactive systems (prostheses, exoskeletons, instrumented objects) to study and characterize the human sensorimotor system, and to improve assistance and rehabilitation of individuals affected by motor skill loss.



Sami Haddadin (M'11) received the Dipl.-Ing. degree in electrical engineering in 2005, the M.Sc. degree in computer science in 2009 from Technical University of Munich (TUM), Munich, Germany, the Honours degree in technology management in 2007 from Ludwig Maximilian University, Munich, Germany, and TUM, and the Ph.D. degree in safety in robotics from RWTH Aachen University, Aachen, Germany, in 2011.

He is currently a Full Professor and the Director of the Institute of Automatic Control, Leibniz University Hannover, Hanover, Germany. He organized/edited several international robotics conferences and journals and published more than 140 scientific articles. His research interests include physical human–robot interaction, nonlinear robot control, real-time motion planning, real-time task and reflex planning, robot learning, optimal control, human motor control, variable impedance actuation, and safety in robotics.

Dr. Haddadin received numerous awards at the top international robotics conferences and journals. Among other things, he received the 2015 IEEE/RAS Early Career Award, the 2015 RSS Early Career Spotlight, the 2015 Alfred Krupp Award, the 2017 Deutscher Zukunftspreis (German Presidents Award for Innovation in Science and Technology), and was selected in 2015 and 2016 as Capital Young Elite Leader under 40 in Germany for the domain "Politics, State, & Society."



Alin Albu-Schäeffler (M'93) received the M.S. degree in electrical engineering from the Technical University of Timișoara, Timișoara, Romania, in 1993 and the Ph.D. degree in automatic control from the Technical University of Munich, Munich, Germany, in 2002.

Since 2012, he has been the Head of the Institute of Robotics and Mechatronics, German Aerospace Center (DLR), which he joined in 1995 as a Ph.D. candidate. Moreover, he is a Professor with the Technical University of Munich, holding the Chair for

“Sensor Based Robotic Systems and Intelligent Assistance Systems” with the Computer Science Department. His personal research interests include robot design, modeling and control, nonlinear control, flexible joint and variable compliance robots, impedance and force control, physical human–robot interaction, bioinspired robot design and control.

Dr. Albu-Schäeffler received several awards, including the IEEE King-Sun Fu Best Paper Award of the Transactions on Robotics in 2012 and several ICRA and IROS Best Paper Awards as well as the DLR Science Award. He was strongly involved in the development of the DLR light-weight robot and its commercialization through technology transfer to KUKA.



Etienne Burdet (S'92–M'96) received the M.S. degree in mathematics, the M.S. degree in physics, and the Ph.D. degree in robotics, all from ETH-Zurich, Zurich, Switzerland.

He is a Professor and Chair in human robotics with Imperial College London, London, U.K. His main research interest includes human–machine interaction. He uses an integrative approach of neuroscience and robotics to investigate human sensorimotor control, and to design efficient assistive devices and training systems for neuro-rehabilitation, which are tested in

clinical trials.